Supplementary Information for

Access to Tough and Transparent Nanocomposites via Pickering Emulsion Polymerization using Biocatalytic Hybrid Lignin Nanoparticles as Functional Surfactants

Adrian Moreno [a] Mohammad Morsali[a], Jinrong Liu[a] and Mika H. Sipponen[a*]

[a] *Department of Materials and Environmental Chemistry, Stockholm University, 10691, Stockholm (Sweden)*

**Corresponding author:* mika.sipponen@mmk.su.se

This supporting information contains:

Total number of pages: 16

Total number of Figures: 12

Total number of Schemes: 1

Total number of Tables: 12

Table S1 show the main characteristics of lignin colloidal dispersions during and after the two step adsorption immobilization process.

Table S1. Characteristics of the colloidal lignin particles (LNPs) prepared in this work.[a] Data was reproduced from a previous study.[1]

Lignin form	hydrodynamic diameter (nm)	PDI	Zeta potential (mV)
LNPs[b]	97 ± 2.5	0.026 ± 0.010	-29.7 ± 3.8
chi-LNPs[c]	190 ± 2.1	0.24 ± 0.152	+31.9 ± 3.2
GOx-chi-LNPs[d]	215 ± 5.6	0.27 ± 0.096	+41.9 ± 2.0

[a]At least three measurements were completed for each parameter. Error ranges correspond to one standard deviation. [b]Values measured at native pH (3.8). [c]Values measured at pH 4 in 15 mM NaOAc buffer. [d]Values measured at pH 5.5 in 15 mM NaOAc buffer.

Table S2 show GOx activity before (GOx) and after (GOx-chi-LNPs) immobilization step. Scheme 1 show the reaction employed to determine the enzyme activity: The oxidation of D-glucose using hydroquinone as an electron acceptor in the presence of GOx or GOx-chi-LNPs.

Table S2. Comparison of apparent catalytic constants of free and immobilized GOx enzyme at room temperature.[a] Data was reproduced from a previous study.[1]

Enzyme status	K_m(M)	V_{max} (M s^{-1})
Free (GOx)	$(5.70 \pm 0.26) \times 10^{-3}$	2.64×10^{-2}
Immobilized (GOx-chi-CLPs)	$(7.00 \pm 0.23) \times 10^{-3}$	1.92×10^{-2}

[a]At least three measurements were completed for each parameter. Error ranges corresponds to one standard deviation.

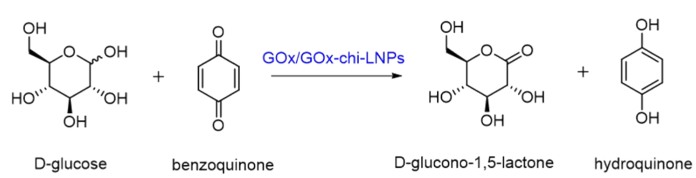

Scheme 1. Oxidation of D-glucose in the presence of hydroquinone catalyzed by GOx or GOx-chiLNPs.

Figure S1 show the evolution of droplet size in Styrene-Pickering emulsions stabilized by GOx-chi-LNPs at different concentration range.

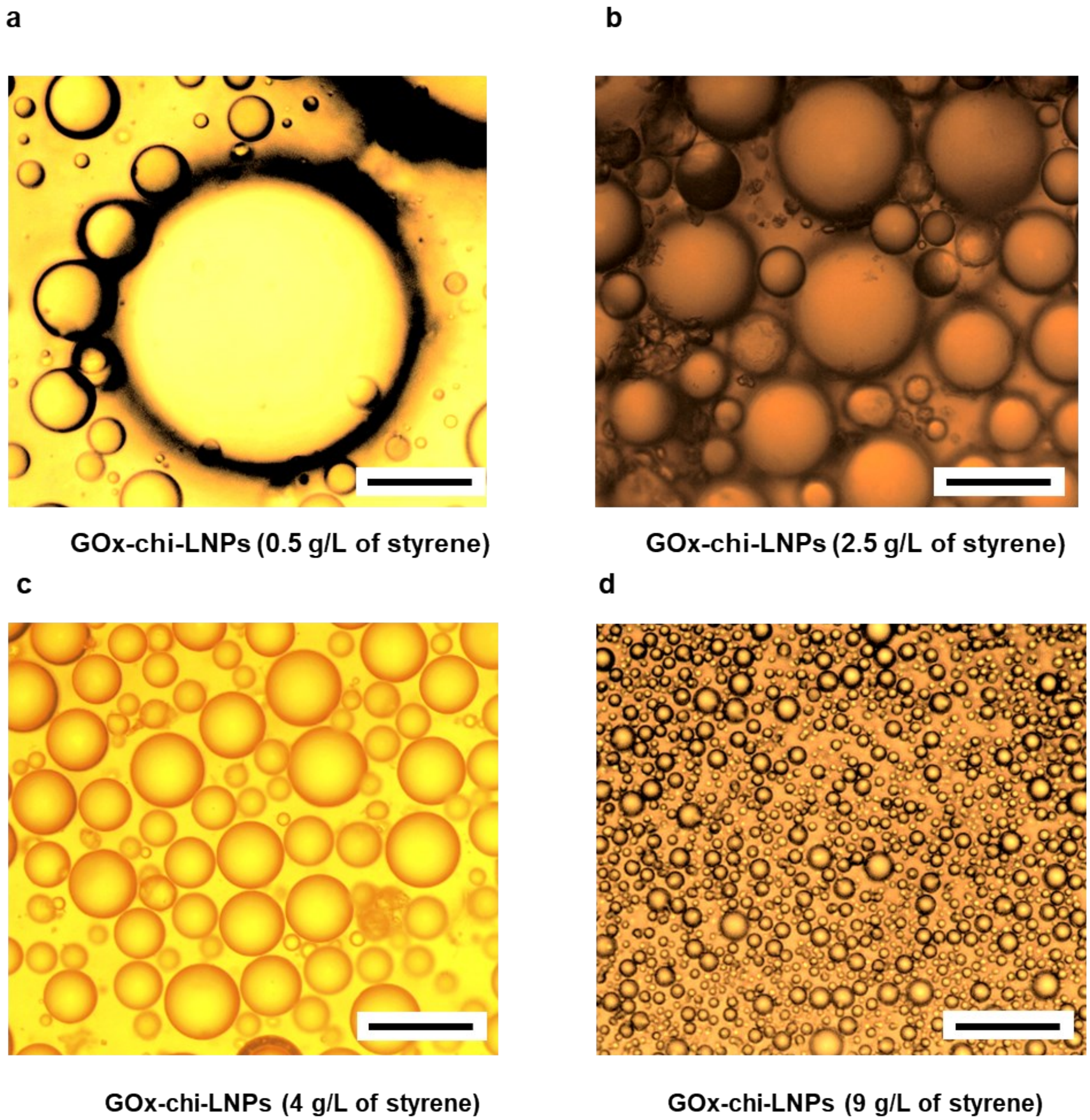

Figure S1. Optical microscope images of Styrene-Pickering emulsions stabilized by GOx-chi-LNPs at different concentrations ranges: (a) 0.5 g of GOx-chi-LNPs per L of styrene, (b) 2.5 g of GOx-chi-LNPs per L of styrene, (c) 4 g of GOx-chi-LNPs per L of styrene and (d) 9 g of GOx-chi-LNPs per L of styrene. Scale bars (100 μm).

Figure S2 show the creaming process present in the emulsions with less amount of GOx-chi-CLPs (a and b) due to a less efficient stabilization process from GOx-chi-LNPs.

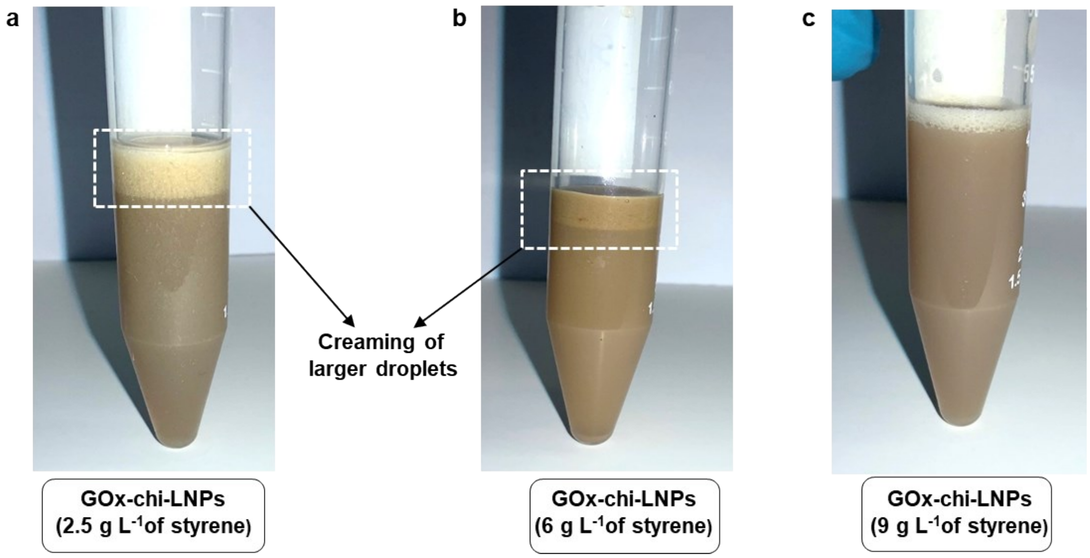

Figure S2. Digital images corresponding to Styrene-Pickering emulsions stabilized by GOx-chi-LNPs at different concentrations ranges: (a) 2.5 g of GOx-chi-LNPs per L of styrene, (b) 6 g of GOx-chi-LNPs per L of styrene, (c) 9 g of GOx-chi-LNPs per L of styrene.

Figure S3 show the digital images corresponding to the latex dispersions obtained after the FRP of Styrene-Pickering emulsions using as stabilizer GOx-chi-LNPs. Figure S3b reveals the coagulum of the latex dispersion due to an insufficient amount of GOx-chi-LNPs, while in Figure S3d a stable latex dispersion was obtained after increase the amount of GOx-chi-LNPs.

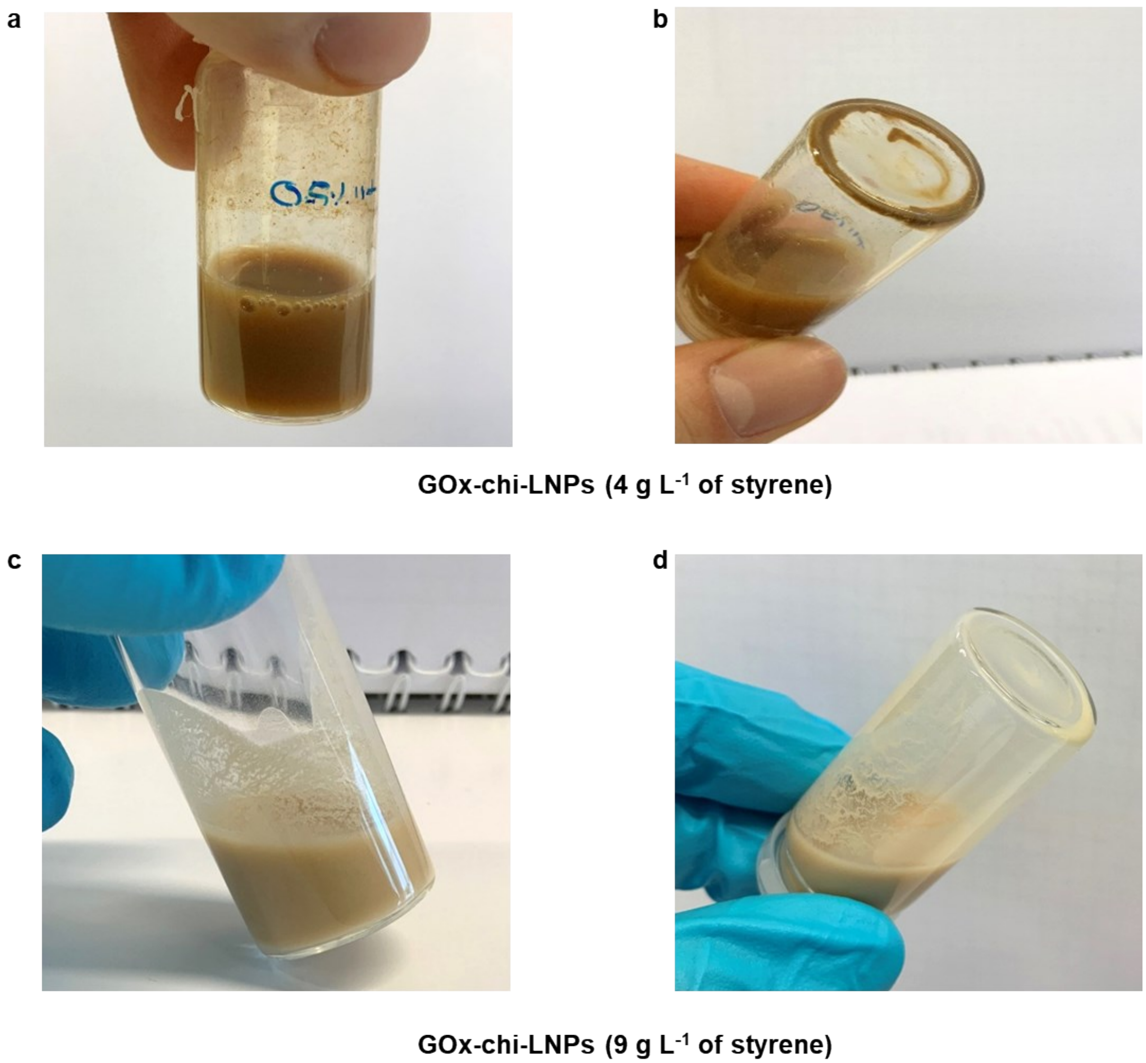

Figure S3. Digital images of Styrene-Pickering emulsions after FRP process stabilized by GOx-chi-LNPs at different concentrations ranges: (a and b) 4 g of GOx-chi-LNPs per L of styrene and (c and d) 9 g of GOx-chi-LNPs per L of styrene.

Figure S4 show the scheme of the enzymatic tandem reaction used to determine the remaining amount of glucose in latex dispersions after the polymerization and the UV-absorbance spectra of oxidized *o*-dianisidine confirming the presence of glucose in the supernatant original sample.

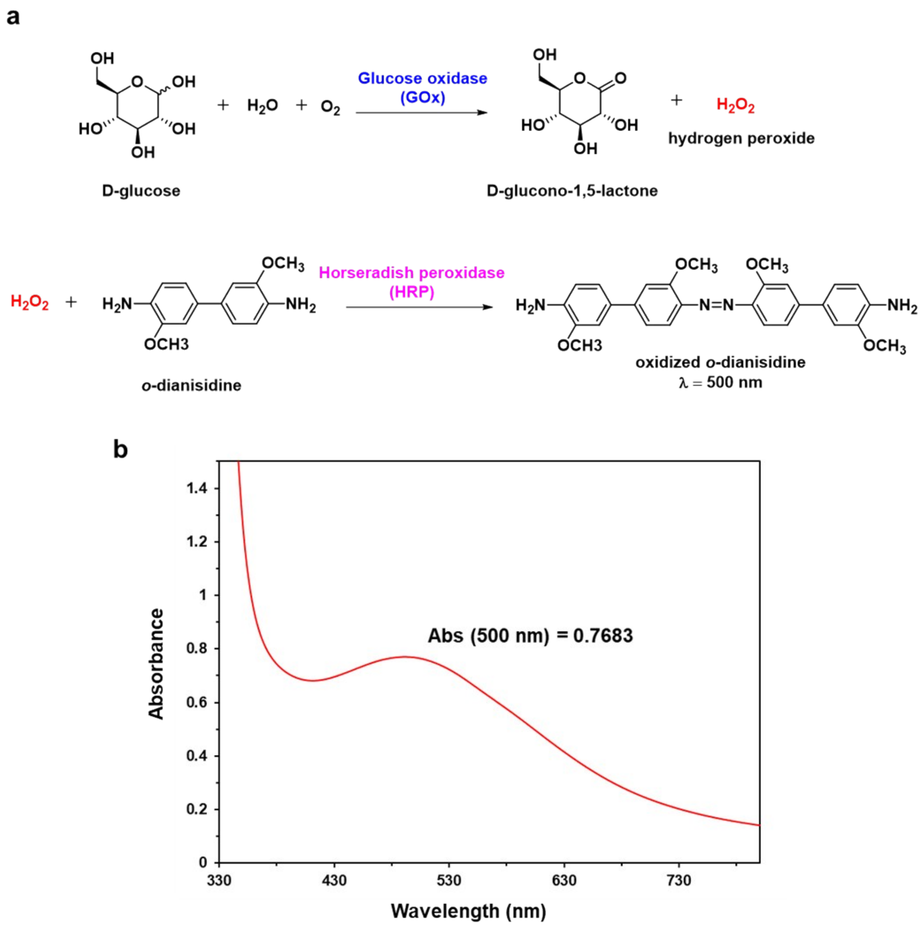

Figure S4. (a) Scheme of enzymatic tandem model reaction used to determine the amount of remaining glucose after the polymerization reaction. (b) UV-visible spectra of reaction mixture showing the formation of the oxidized form of *o*-dianisidine as consequence of the cascade reaction. Reaction conditions: 25 μL of purified supernatant solution from latex dispersions, [GOx] = 15 mg/mL [HRP] = 20 mg/mL and [*o*-dianisidine] = 9.1 mM Reaction media: pH 6 in 15 mM NaOAc buffer. Total volume reaction = 4 mL.

Figure S5 show SEM characterization images of purified PS microparticles after basic treatment. Magnification in b, reveal remaining GOx-chi-LNPs in the surface of the PS microparticle.

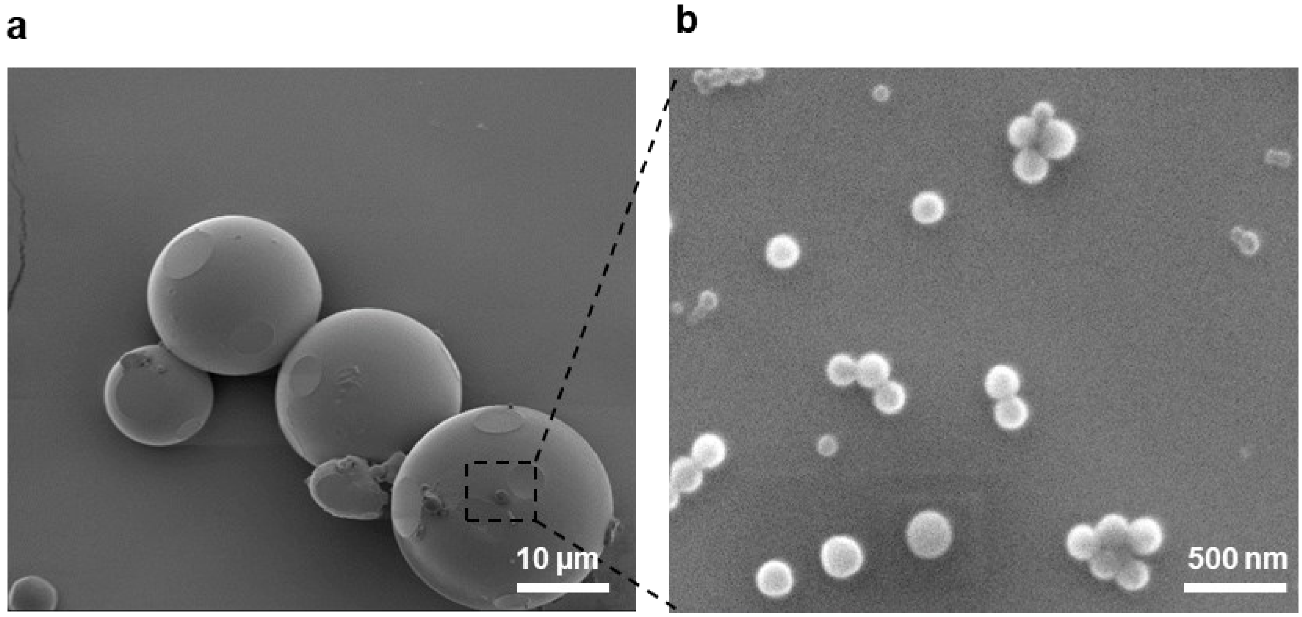

Figure S5. (a and b) SEM images of bare PS microbeads after FRP at 65 ºC and treatment with basic solution (NH_4OH, 35 wt %)

Figure S6 show the TGA analysis of GOx-chi-LNPs-coated PS microparticles before (a and b) and after (c and d) treatment with basic solution (NH_4OH, 35 wt %). Magnification of char residue (7 wt % vs 0.1 wt %) demonstrate an efficient removal of most part of GOx-chi-LNPs after the basic treatment.

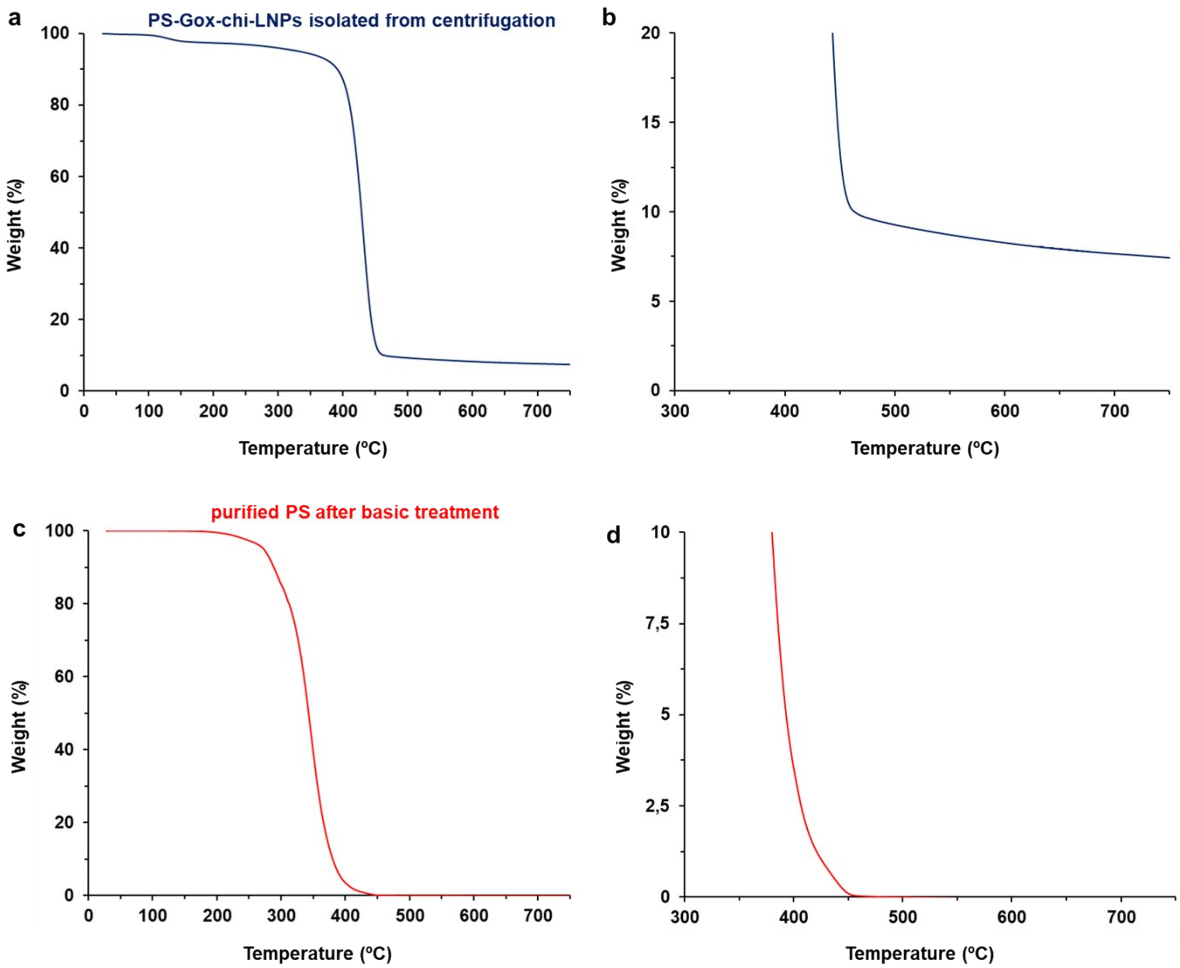

Figure S6. TGA analysis curves for (a) bare PS microparticles and (b) GOx-chi-LNPs coated PS microparticles (GOx-chi-LNPs, 2.5 wt %). (b and d) are magnification of the end thermal residue for bare PS microparticles and GOx-chi-LNPs coated PS microparticles, respectively.

Figure S7 display digital images for de-emulsification in basic conditions, and re-emulsification (by restoring original pH) process for PS-latex dispersions stabilized with GOx-chi-LNPs.

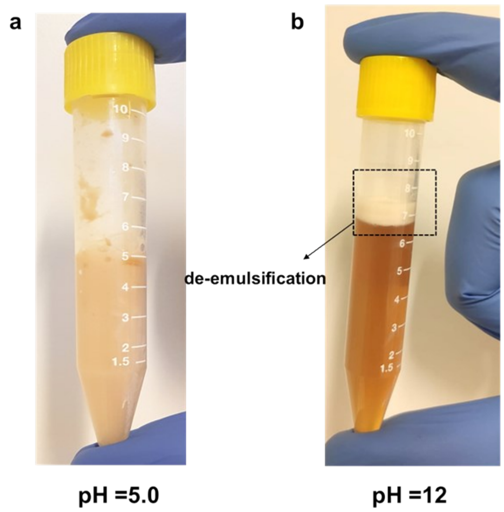

Figure S7. pH-responsive behavior of PS-Pickering emulsion latex dispersion stabilized by GOx-chi-LNPs (5 wt %).

Figure S8 show the appearance of PS latex dispersion stabilized with GOx-chi-LNPs (2.5 and 15 wt %) before (a and c), and after melting process at 160 ºC (b and d).

Figure S8. Digital images of GOx-chi-LNPs-PS particles (a and c) isolated from latex dispersion (2.5 and 15 wt%, respectively). (b and d) Digital images of PS-GOx-chi-LNPs composite film obtained after melt-pressing process of particles shown on (a and c).

Figure S9 show the morphology and distribution of GOx-chi-LNPs in PBMA-GOx-chi-LNPs composite films with 2.5 and 15 wt % of GOx-chi-LNPs, respectively.

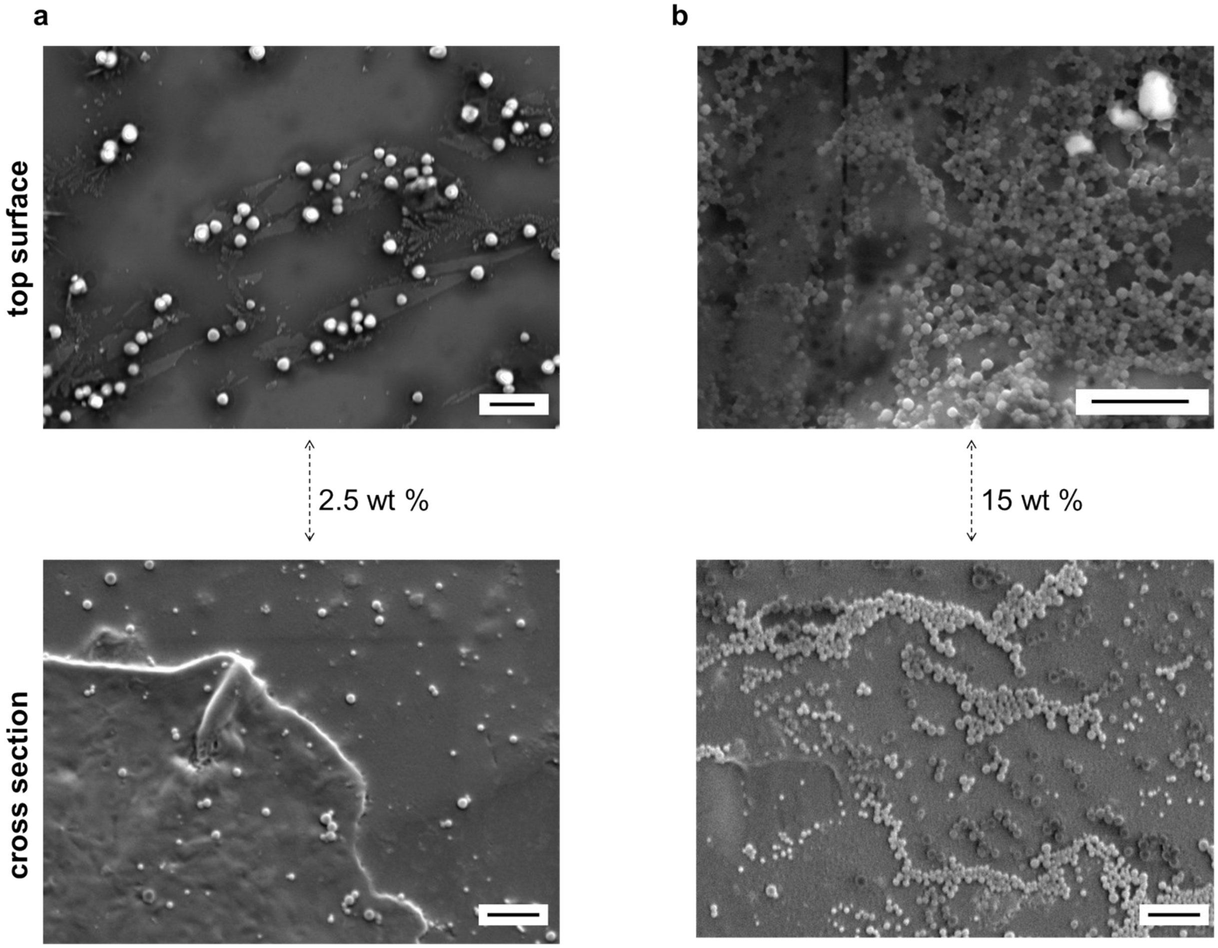

Figure S9. SEM micrographs of top and cross-sectional surfaces of PBMA-GOx-chi-LNPs composites films at: (a) GOx-chi-LNPs 2.5 wt % (b) GOx-chi-LNPs 15 wt %. Scale bars (1 μm)

Table S3 and S4 summarize the mechanical properties of PS- and PBMA-GOx-chi-LNPs composites.

Table S3. Mechanical properties for PS and PS-GOx-chi-LNPs composites

Material	Young's modulus (MPa)	Tensile stress (MPa)	Strain at break (%)	Toughness (MJ/m^3)
PS	1484.5 ± 81.7	12.3 ± 1.72	1.31 ± 0.35	0.10 ± 0.03
PS-GOx-chi-$LNPs_{2.5}$	1863.7 ± 114.3	21.8 ± 2.26	1.77 ± 0.34	0.24 ± 0.03
PS-GOx-chi-$LNPs_{5}$	2308.9 ± 72.3	23.1 ± 1.16	1.63 ± 0.12	0.27 ± 0.02
PS-GOx-chi-$LNPs_{10}$	2627.6 ± 116.2	26.6 ± 1.19	1.63 ± 0.04	0.29 ± 0.01
PS-GOx-chi-$LNPs_{15}$	3050.4 ± 120.0	29.8 ± 1.96	1.69 ± 0.31	0.35 ± 0.02
PS-GOx-chi-$LNPs_{20}$	2354.3 ± 149.7	21.4 ± 0.97	1.35 ± 0.30	0.21 ± 0.03
PS-GOx-chi-$LNPs_{30}$	2148.4 ± 115.1	22.2 ± 1.33	1.74 ± 0.03	0.26 ± 0.01

Table S4. Mechanical properties of PBMA and PBMA-GOx-chi-LNPs composites

Material	Young's modulus (MPa)	Tensile stress (MPa)	Strain at break (%)	Toughness (MJ/m^3)
PBMA	0.92 ± 0.05	0.24 ± 0.05	316.3 ± 61.9	0.53 ± 0.16
PBMA-GOx-chi-$LNPs_{2.5}$	2.6 ± 0.50	0.69 ± 0.26	398.1 ± 29.8	1.67 ± 0.47
PBMA-GOx-chi-$LNPs_{5}$	5.0 ± 0.22	0.87 ± 0.12	375.4 ± 45.6	2.14 ± 0.31
PBMA-GOx-chi-$LNPs_{10}$	8.2 ± 0.97	1.58 ± 0.11	381.4 ± 55.1	4.13 ± 0.53
PBMA-GOx-chi-$LNPs_{15}$	12.6 ± 1.41	3.36 ± 0.31	334.2 ± 23.1	8.04 ± 1.37
PBMA-GOx-chi-$LNPs_{20}$	8.7 ± 1.04	2.16 ± 0.11	338.4 ± 8.8	5.41 ± 1.29
PBMA-GOx-chi-$LNPs_{30}$	7.7 ± 0.40	2.07 ± 0.22	329.2 ± 28.7	5.18 ± 1.31

Table S5-S12 summarize statistical analysis of PS- and PBMA-GOx-chi-LNPs provided by one-way analysis of variance (ANOVA) with Tukey's honest significant difference (HSD) all-pairwise comparison test at a significance level of $p < 0.05$. The results summarized indicate that the introduction of GOx-chi-LNPs into the polymeric matrix (15 wt %) improve significantly the mechanical properties in both cases (PS and PBMA) in comparison to pristine polymeric materials.

Table S5. Statistical analysis of Young's modulus values of PS and PS-GOx-chi-LNPs composite films. One-way ANOVA with Tukey's honest significant difference (HSD) all-pairwise comparison test ($p<0.05$). df = 6 (between) and 21 (within), F=106.79 Italic letters *a–f* indicates statistically significant difference between different groups.

Material	PS	PS-GOx-chi-LNPs$_{2.5}$	PS-GOx-chi-LNPs$_{5}$	PS-GOx-chi-LNPs$_{10}$	PS-GOx-chi-LNPs$_{15}$	PS-GOx-chi-LNPs$_{20}$	PS-GOx-chi-LNPs$_{30}$
Group	*a*	*b*	*c*	*d*	*e*	*c*	*f*

Table S6. Statistical analysis of tensile strength values of PS and PS-GOx-chi-LNPs composite films. One-way ANOVA with Tukey's honest significant difference (HSD) all-pairwise comparison test ($p<0.05$). df = 6 (between) and 21 (within), F=44.96 Italic letters *a–d* indicates statistically significant difference between different groups.

Material	PS	PS-GOx-chi-LNPs$_{2.5}$	PS-GOx-chi-LNPs$_{5}$	PS-GOx-chi-LNPs$_{10}$	PS-GOx-chi-LNPs$_{15}$	PS-GOx-chi-LNPs$_{20}$	PS-GOx-chi-LNPs$_{30}$
Group	*a*	*b*	*b*	*c*	*d*	*b*	*b*

Table S7. Statistical analysis of strain at failure values of PS and PS- GOx-chi-LNPs composite films. One-way ANOVA with Tukey's honest significant difference (HSD) all-pairwise comparison test ($p<0.05$). df = 6 (between) and 21 (within), F=2.14 Italic letters *a–d* indicates statistically significant difference between different groups.

Material	PS	PS-GOx-chi-LNPs$_{2.5}$	PS-GOx-chi-LNPs$_{5}$	PS-GOx-chi-LNPs$_{10}$	PS-GOx-chi-LNPs$_{15}$	PS-GOx-chi-LNPs$_{20}$	PS-GOx-chi-LNPs$_{30}$
Group	*ad*	*b*	*bc*	*b*	*b*	*ad*	*b*

Table S8. Statistical analysis of toughness values of PS and PS-GOx-chi-LNPs composite films. One-way ANOVA with Tukey's honest significant difference (HSD) all-pairwise comparison test ($p<0.05$). df = 6 (between) and 21 (within), F=40.75 Italic letters *a–g* indicates statistically significant difference between different groups.

Material	PS	PS-GOx-chi-LNPs$_{2.5}$	PS-GOx-chi-LNPs$_{5}$	PS-GOx-chi-LNPs$_{10}$	PS-GOx-chi-LNPs$_{15}$	PS-GOx-chi-LNPs$_{20}$	PS-GOx-chi-LNPs$_{30}$
Group	*a*	*b*	*c*	*d*	*e*	*f*	*bg*

Table S9. Statistical analysis of Young's modulus values of PBMA and PBMA-GOx-chi-LNPs composite films. One-way ANOVA with Tukey's honest significant difference (HSD) all-pairwise comparison test ($p<0.05$). df = 6 (between) and 28 (within), F=124.05 Italic letters *a–e* indicates statistically significant difference between different groups.

Material	PBMA	PBMA-GOx-chi-$LNPs_{2.5}$	PBMA-GOx-chi-$LNPs_{5}$	PBMA-GOx-chi-$LNPs_{10}$	PBMA-GOx-chi-$LNPs_{15}$	PBMA-GOx-chi-$LNPs_{20}$	PBMA-GOx-chi-$LNPs_{30}$
Group	*a*	*b*	*c*	*d*	*e*	*d*	*d*

Table S10. Statistical analysis of tensile strength values of PBMA and PBMA-GOx-chi-LNPs composite films. One-way ANOVA with Tukey's honest significant difference (HSD) all-pairwise comparison test ($p<0.05$). df = 6 (between) and 28 (within), F=54.16 Italic letters *a–e* indicates statistically significant difference between different groups.

Material	PBMA	PBMA-GOx-chi-$LNPs_{2.5}$	PBMA-GOx-chi-$LNPs_{5}$	PBMA-GOx-chi-$LNPs_{10}$	PBMA-GOx-chi-$LNPs_{15}$	PBMA-GOx-chi-$LNPs_{20}$	PBMA-GOx-chi-$LNPs_{30}$
Group	*a*	*b*	*b*	*c*	*d*	*e*	*e*

Supplementary Table 11. Statistical analysis of strain at failure values of PBMA and PBMA-GOx-chi-LNPs composite films. One-way ANOVA with Tukey's honest significant difference (HSD) all-pairwise comparison test ($p<0.05$). df = 6 (between) and 28 (within), F=3.37 Italic letters *a–d* indicates statistically significant difference between different groups.

Material	PBMA	PBMA-GOx-chi-$LNPs_{2.5}$	PBMA-GOx-chi-$LNPs_{5}$	PBMA-GOx-chi-$LNPs_{10}$	PBMA-GOx-chi-$LNPs_{15}$	PBMA-GOx-chi-$LNPs_{20}$	PBMA-GOx-chi-$LNPs_{30}$
Group	*a*	*b*	*bc*	*b*	*ad*	*ad*	*a*

Supplementary Table 12. Statistical analysis of toughness values of PBMA and PBMA-GOx-chi-LNPs composite films. One-way ANOVA with Tukey's honest significant difference (HSD) all-pairwise comparison test ($p<0.05$). df = 6 (between) and 28 (within), F=35.53 Italic letters *a–e* indicate statistically significant difference between different groups.

Material	PBMA	PBMA-GOx-chi-$LNPs_{2.5}$	PBMA-GOx-chi-$LNPs_{5}$	PBMA-GOx-chi-$LNPs_{10}$	PBMA-GOx-chi-$LNPs_{15}$	PBMA-GOx-chi-$LNPs_{20}$	PBMA-GOx-chi-$LNPs_{30}$
Group	*a*	*b*	*b*	*c*	*d*	*e*	*ce*

Figure S10 show an effective decolorization of ABTS $^{\bullet+}$ solution (antioxidant scavenging effect) during time in the presence of PBMA-GOx-chi-LNPs$_{10}$.

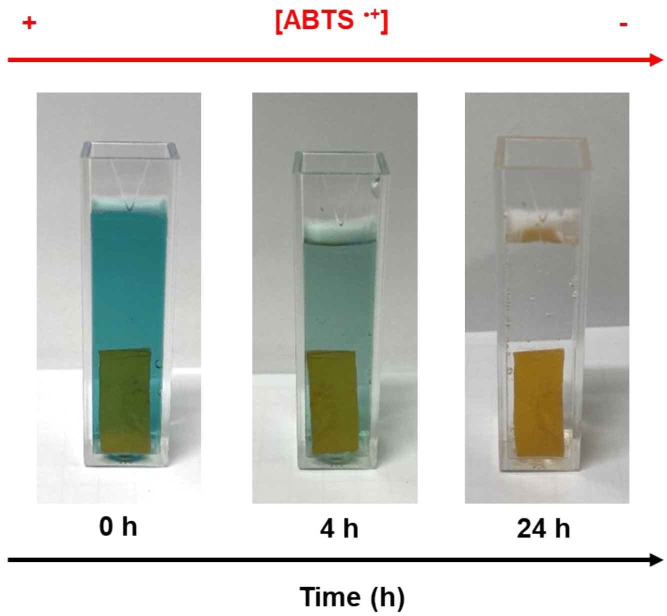

Figure S10. Representative digital images taken at different time periods during the antioxidant scavenging of ABTS $^{\bullet+}$ solution from PBMA-GOx-chi-LNPs$_{10}$ composite film

Figure S11 show the evaluation of mechanical properties of PBMA-GOx-chi-LNPs$_{10}$ composites after antioxidant assay employing ABTS $^{\bullet+}$ solution as source of active radicals.

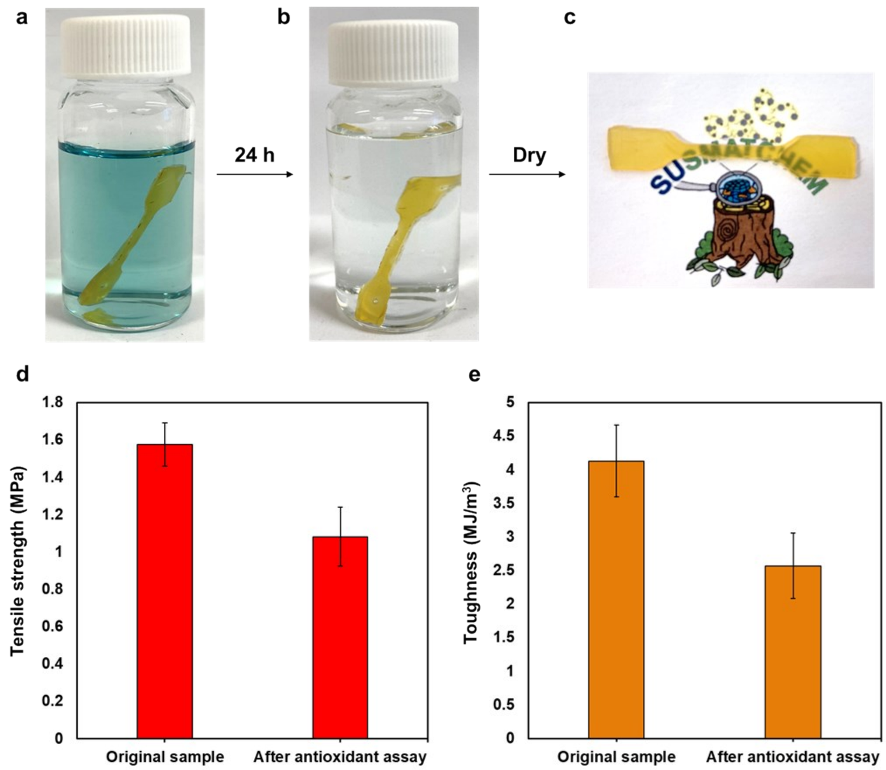

Figure S11. Digital images (a, b and c) taken at different time periods during the antioxidant assay from PBMA-GOx-chi-LNPs$_{10}$ composite film. Mechanical properties of PBMA-GOx-chi-LNPs$_{10}$ composites: (d) Tensile strength and (e) Toughness before and after the antioxidant assay. In (d and e), the error bars represent ± standard deviation (SD) from the mean values (n=5).

Figure S12 show the possibility to reuse PBMA-GOx-chi-LNPs$_{10}$ composite film by melting process.

Figure S12. (a) PBMA-GOx-chi-LNPs10 composite film. (b) PBMA-Gox-chi-LNPs10 film after tensile test. (c) PBMA-GOx-chi-LNPs10 composite film after recycling by melting process from specimen displayed in b.

References

[1]A. Moreno and M. H. Sipponen, *Nat. Commun.* 2020, **11**, 5599.